Can few-shot learning methods segment global-sclerotic glomeruli in WSI?

Márcio dos Santos*, Luiz Souza*§, Jefferson Fontinele*†, Marcelo Mendonça*‡, Angelo Duarte¶, Washington LC dos-Santos‖ and Luciano Oliveira*‖
*Intelligent Vision Research Lab, Institute of Computing, Federal University of Bahia
Email: santosmarcio,lrebouca{@ufba.br}
§Federal Institute of Maranhao
Email: luiz.otavio{@ifma.edu.br}
†Federal University of Maranhao
Email: jefferson.fs{@ufma.br}
‡Federal Institute of Bahia
Email: marcelomendonca{@ifba.edu.br}
¶High-Performance Computing Lab, Department of Technology, State University of Feira de Santana
Email: angeloduarte@uefs.br
‖Structural and Molecular Pathology Lab, Gonçalo Moniz Institute, Fundação Oswaldo Cruz
Email: wluis@bahia.fiocruz.br

Abstract*—Glomeruli are central to the analysis of whole slide images (WSIs) in kidney biopsies, as they are affected by a wide range of lesions that reflect both causes and consequences of renal diseases. In automated WSI analysis using machine learning, glomeruli are typically the first regions to be segmented or detected, enabling subsequent diagnostic tasks. The Bowman's capsule (BC) usually serves as the primary anatomical marker, delineating the glomerulus from the surrounding interstitium. While this boundary is preserved in normal and partially sclerotic glomeruli, globally sclerotic glomeruli often lose the BC, appearing visually borderless and posing a major challenge for automatic detection. In recent years, several studies have addressed glomerulus segmentation; however, few have focused on the specific challenge of globally sclerotic glomeruli, often analyzing them only in isolated per-cropped images. In this work, we present a comparative evaluation of four few-shot semantic segmentation (FSS) methods: DMACA, VAT, HSNet, and PMNet. These approaches aim to learn from only a few labeled examples, addressing the data scarcity of globally sclerotic glomeruli. These methods were applied to three classes of glomeruli: those with well-defined borders, partially borderless glomeruli, and globally sclerotic borderless glomeruli, using the Dice metric. Our results highlight the intrinsic difficulty of segmenting globally sclerotic glomeruli from WSIs, with a mean Dice score across all the evaluated methods of only 0.02 when evaluated at the whole-slide level. In contrast, per-crop evaluations yielded markedly higher performance, with mean Dice scores reaching 0.93 for globally sclerotic glomeruli.

I. Introduction

A kidney biopsy is a medical procedure in which a small specimen of kidney tissue is obtained from a human for microscopic investigation. This procedure is typically performed to diagnose and evaluate several kidney diseases (*e.g.*, nephritis syndrome and nephrotic syndrome). This procedure allows nephrologists and pathologists to examine the structure of kidney tissue under a microscope or scanned samples, allowing the display of gigapixel whole slide images (WSIs) [1]–[3]. Among the structures present in the human kidney biopsy, the glomerulus – situated within each kidney nephron – is responsible for the blood filtration process to form urine.

Fig. 1 illustrates representative glomeruli in WSIs: (a) a healthy glomerulus (normal), (b) a partially sclerotic glomerulus (segmental sclerosis), and (c) a global sclerotic glomerulus. While normal and segmentally sclerotic glomeruli preserve the Bowman's capsule to some extent and retain key histological primitives, globally sclerotic glomeruli are completely fibrotic, with indistinct boundaries and severe structural degradation [4]. Notably, in this last case, even visual identification is challenging due to the lack of clear contours separating the glomerulus from surrounding tissue.

Glomerulus segmentation has emerged as one of the first tasks addressed by machine learning-based expert systems in computational nephropathology [5]. The primary target is to provide specialists with a decision-making tool for pre-screening WSIs (*e.g.*, glomerulus counting), thereby streamlining subsequent automated tasks (*e.g.*, glomerular lesion classification). To understand how segmentation has been explored in renal pathology, we reviewed related works using three main criteria: (i) Whether the work addressed glomerulus segmentation, (ii) whether it relied on whole-slide images, even if analysis was performed on cropped regions, and (iii) whether it was indexed in PubMed[1], the main repository of peer-reviewed medical literature. Many of these studies do not distinguish between different types of glomeruli, focusing instead on developing robust segmenters for a canonical glomerular structure [6]–[11]. With the exception of [10], which introduces a tailored deep learning network for a

[1]https://pubmed.ncbi.nlm.nih.gov

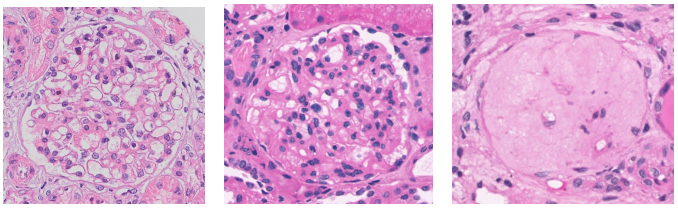

(a) (b) (c)

Fig. 1. Examples of glomeruli from the WSI data sets. (a) Normal, (b) segmental sclerosis, and (c) global sclerosis.

more complex segmentation task, most approaches report Dice scores above 0.90 by applying off-the-shelf (or slightly modified) methods, typically on WSIs stained with HE, PAS, or PAMS.

Despite these advances, the literature remains limited when it comes to pathological variability. In particular, segmentation is often simplified by targeting glomeruli with clear borders, while the more complex cases of partially or globally sclerotic glomeruli are overlooked. Some studies address the binary classification of normal versus sclerotic glomeruli [12]–[18], yet they seldom report performance separately for each class. As a result, the apparent high scores are likely inflated by dataset imbalance, since normal glomeruli vastly outnumber sclerotic ones.

Only a handful of works have specifically investigated global glomerulosclerosis [5], [19], [20], but relevant limitations persist. Jiang et al. [5] compare globally sclerotic glomeruli with normal and other types, relying on large, manually curated patches, which naturally facilitates segmentation accuracy. Yu et al. [19] develop a framework for multi-structure segmentation in WSIs, but it remains unclear whether globally sclerotic glomeruli are explicitly targeted, despite their results suggesting unexpectedly high performance. More recently, Wang et al. [20] propose Glo-Net, a dual-task network evaluated on multiple datasets, reporting strong performance (mIoU $>$ 0.8) even for globally sclerotic glomeruli. However, such results raise questions about preprocessing strategies and whether the true difficulty of segmenting these borderless structures is being fully captured.

While previous works have advanced the segmentation of well-defined glomeruli, globally sclerotic glomeruli remain an open challenge. This paper addresses this gap by applying few-shot semantic segmentation (FSS) methods to investigate the problem at both the WSI and per-crop levels, considering limited data availability, time-consuming annotation workload, and severe class imbalance.

II. Materials and Methods

A. General approach for glomerulus segmentation

A general pipeline for the automated segmentation of glomeruli in WSIs is illustrated in Fig. 2. Designed to mirror a real clinical diagnostic workflow, the process is fully automated and requires no manual intervention. The method begins by processing each WSI using a sliding-window approach,

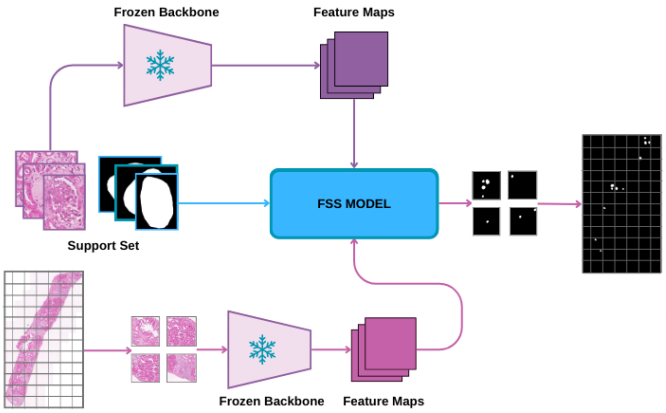

Fig. 2. General pipeline of prominent few-shot segmentation models for processing WSIs.

TABLE I
Summary of the characteristics of the datasets.

Data set	Stain	# WSI		# Glom.		# Classes		
		Train	Test	Train	Test	Normal	Segmental	Global
Normal	HE	12	3	181	38	219	-	-
	PAS	12	3	180	31	211	-	-
	PAMS	12	3	180	33	213	-	-
	ALL	36	9	541	102	643	-	-
Sclerosis	HE	-	19	-	72	-	48	24
	PAS	-	18	-	76	-	56	20
	ALL	-	37	-	148	-	104	44
Mixed	HE	1	-	12	-	4	4	4

which extracts patches of 1024×1024 pixels. To mitigate border effects and preserve contextual information, each patch includes a padding of 256×256 pixels. These patches are then resized to 384×384 pixels to reduce computational cost.

Subsequently, each patch is fed into a frozen backbone network to generate dense feature maps. To ensure representation consistency, the same backbone is used for both query and support images. These feature maps are then processed by the few-shot segmentation models to produce a preliminary prediction for each patch. Finally, the individual patch-level predictions are aggregated and stitched together to form the high-resolution segmentation mask for the entire WSI, enabling the comprehensive and automated identification of glomeruli.

B. Datasets

The dataset compilation used in this paper originates from two sets named Normal and Sclerosis. The **Normal** dataset extends the prior ANONYMOUS dataset, now featuring 45 kidney WSIs collected from 5 patients. The **Sclerosis** dataset contains 37 kidney sections from 33 patients. The **Mixed** dataset contains a single WSI from 1 patient, in which glomeruli were annotated into three classes (normal, segmental sclerosis, and global sclerosis). This slide was used exclusively for training the FSS models and for per-crop evaluation through 12 manually extracted patches (4 per class). The renal biopsies used to build the dataset were fixed in formalin-acetic acid-alcohol to preserve their histological structure, later in-

TABLE II

COMPARISON OF RESULTS (μDICE SCORE) OBTAINED FROM FOUR SEGMENTATION NETWORKS ON **WSI-LEVEL** AND **CROPPED** GLOMERULI, ACROSS THE THREE CLASSES: NORMAL, SEGMENTAL SCLEROSIS, AND GLOBAL SCLEROSIS.

Models	**Normal**				**Segmental**			**Global**		
WSI	**HE**	**PAS**	**PAMS**	**ALL**	**HE**	**PAS**	**ALL**	**HE**	**PAS**	**ALL**
DMACA	0.79 ± 0.00	0.87 ± 0.01	0.84 ± 0.02	**0.86 ± 0.03**	0.16 ± 0.11	0.23 ± 0.14	0.23 ± 0.15	0.00 ± 0.01	0.00 ± 0.01	0.00 ± 0.01
VAT	**0.80 ± 0.02**	0.84 ± 0.04	**0.91 ± 0.03**	**0.86 ± 0.03**	**0.17 ± 0.12**	**0.24 ± 0.14**	**0.26 ± 0.17**	**0.02 ± 0.04**	**0.02 ± 0.04**	0.00 ± 0.01
HSNet	0.62 ± 0.02	0.55 ± 0.04	0.53 ± 0.01	0.75 ± 0.07	0.09 ± 0.08	0.10 ± 0.07	0.18 ± 0.12	0.02 ± 0.05	0.00 ± 0.00	**0.02 ± 0.05**
PMNet	0.77 ± 0.01	**0.88 ± 0.03**	0.90 ± 0.01	0.86 ± 0.05	0.09 ± 0.07	0.13 ± 0.10	0.15 ± 0.11	0.00 ± 0.00	0.01 ± 0.01	0.00 ± 0.00
Models	**Normal**				**Segmental**			**Global**		
Crop	**HE**	**PAS**	**PAMS**	**ALL**	**HE**	**PAS**	**ALL**	**HE**	**PAS**	**ALL**
DMACA	0.94 ± 0.04	0.96 ± 0.02	0.96 ± 0.03	0.96 ± 0.03	0.91 ± 0.04	0.88 ± 0.06	0.92 ± 0.04	0.85 ± 0.05	0.84 ± 0.07	0.88 ± 0.05
VAT	0.95 ± 0.04	**0.97 ± 0.02**	**0.97 ± 0.02**	0.96 ± 0.03	0.92 ± 0.06	0.94 ± 0.05	0.94 ± 0.04	0.91 ± 0.04	**0.92 ± 0.03**	**0.93 ± 0.03**
HSNet	0.94 ± 0.05	0.96 ± 0.02	0.96 ± 0.03	0.96 ± 0.03	**0.94 ± 0.03**	**0.94 ± 0.03**	**0.95 ± 0.03**	**0.92 ± 0.04**	0.91 ± 0.04	0.92 ± 0.04
PMNet	**0.95 ± 0.04**	**0.97 ± 0.02**	0.97 ± 0.03	**0.96 ± 0.02**	0.92 ± 0.04	0.87 ± 0.07	0.89 ± 0.06	0.84 ± 0.07	0.79 ± 0.09	0.77 ± 0.13

cluded in paraffin, and sectioned at 2 µm. WSIs were digitized using a VS 110 Olympus scanner with 40× magnification for the Normal dataset, and a Zeiss Imager Z2 scanner with 20× magnification for the Sclerosis and Mixed datasets. The main characteristics of these datasets are summarized in Table I.

C. Evaluated FSS Methods

Few-shot semantic segmentation (FSS) aims to segment objects of previously unseen classes using a query image along with a small set of annotated examples. This capability is particularly valuable in our case, where annotated data of globally sclerotic glomeruli in WSIs is scarce. In a k-shot setting, given a query image I_q and a support set $S = \{(I_s^i, M_s^i)\}_{i=1}^k$, where each pair (I_s^i, M_s^i) consists of a support image and its corresponding ground-truth mask, the objective is to predict the segmentation mask M_q of the query image I_q.

Despite architectural differences, FSS models follow a consistent pipeline (see Fig. 2): Feature extraction using pretrained backbones, cross-image correspondence establishment, and mask generation via learnable decoders. For our evaluation, we selected four representative FSS approaches that exemplify different paradigms in correspondence modeling and mask refinement. **HSNet** [21] captures dense pixel-wise relationships through multi-level 4D correlations; **DCAMA** [22] employs an attention mechanism incorporating foreground and background support information; **PMNet** [23] refines pixel-to-patch affinities and enhances coarse masks via spatial filtering; and **VAT** [24] combines local and global context using volumetric convolutional and transformer modules. Together, these methods exemplify diverse state-of-the-art FSS strategies.

D. Implementation Details

We used official model implementations with default parameters, employing ResNet-101 (ImageNet-1K pretrained) for HSNet and VAT, and Swin Transformer (SwinB) with ImageNet pretraining for DCAMA and PMNet. All models were trained for 300 epochs on NVIDIA RTX 4090 GPU with AMD Ryzen 9 7900X3D CPU using batch size 8, a warm-up learning rate scheduler peaking at 1×10^{-4}, and frozen backbone weights to preserve pretrained features, with online augmentations applied to improve generalization. Training followed an episodic paradigm, in which each episode $\mathcal{E} = (\mathcal{S}, \mathcal{Q})$ consisted of a support set $\mathcal{S} = \{(I_s, M_s)\}$ and a query pair $\mathcal{Q} = (I_q, M_q)$ sampled from the training subset of the Normal dataset. For evaluation, we employed a 12-shot setting with support sets comprising 12 Mixed dataset crops (4 normal, 4 segmental sclerosis, and 4 global sclerosis), maintaining this configuration for both whole slide image patches and individual cropped glomeruli experiments.

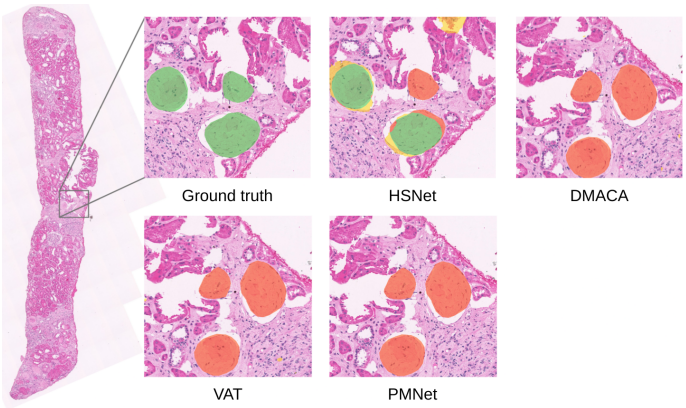

Fig. 3. Comparison of visual results produced by the FSS models on a WSI exhibiting global sclerosis glomeruli. The yellow mask is false-positive pixels, the red mask is false-negative pixels, and the green mask is true-positive pixels

III. RESULTS

Our experimental evaluation highlights substantial performance gaps between WSI-level and per-crop segmentation, with notable variation across glomerular pathology types. Table II reports the quantitative results for models trained both per-stain and across all stains, evaluated using the Dice coefficient. Dice was selected as the primary metric due to its sensitivity to small and morphologically ambiguous structures. By prioritizing true positives and penalizing false negatives, it provides a more reliable measure for sclerotic glomeruli compared to IoU, which is more influenced by false positives.

A. WSI-Level Segmentation Performance

For normal glomeruli, the models achieved moderate to good results, with mean Dice scores between 0.75 and 0.86 across all stain types. DMACA, VAT, and PMNet performed similarly (0.86 ± 0.03 each), while HSNet lagged slightly

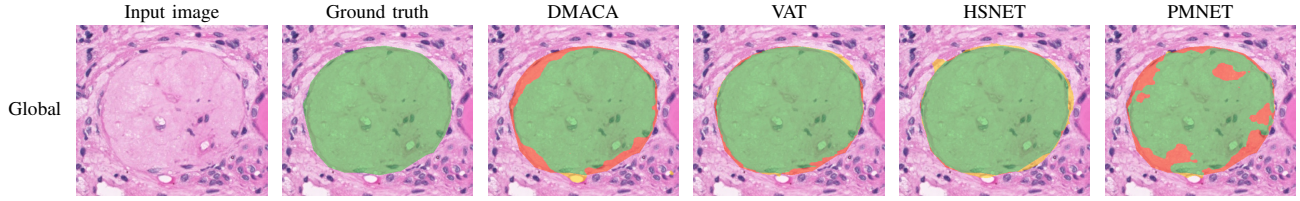

Fig. 4. From left to right: Input image, ground truth, and results from DMACA, VAT, HSNET and PMNET considering per-crop segmentation using HE stain for global glomeruli. The yellow mask is false-positive pixels, the red mask is false-negative pixels, and the green mask is true-positive pixels (best view in colors).

(0.75 ± 0.07). Performance varied notably with staining, with PAMS consistently yielding the best results, followed by PAS and HE. In contrast, segmentally sclerotic glomeruli were far more challenging to segment, with Dice scores dropping to 0.15–0.26. VAT reached the highest performance (0.26 ± 0.17), followed by DMACA (0.23 ± 0.15), HSNet (0.18 ± 0.12), and PMNet (0.15 ± 0.11). The large standard deviations indicate high variability in segmentation quality across different cases.

Global sclerotic glomeruli segmentation at the WSI level proved extremely challenging for all evaluated methods. Performance was near-zero across all approaches, with Dice scores effectively at 0.00 ± 0.01 for most method-stain combinations. These results underscore the fundamental difficulty of segmenting borderless, globally sclerotic structures in the complex context of whole slide images.

B. Per-Crop Segmentation Performance and Clinical Implications

While per-crop evaluation revealed substantially improved performance across all glomerular types and methods, these results must be interpreted with caution regarding clinical applicability. For normal glomeruli, all four methods achieved excellent performance, with mean Dice scores consistently above 0.94. Similarly high performance was observed for segmentally sclerotic glomeruli, with mean Dice scores ranging from 0.89 to 0.95, led by HSNet (0.95 ± 0.03).

Most notably, globally sclerotic glomeruli showed high performance in per-crop evaluation, with VAT achieving 0.93 ± 0.03, followed by HSNet (0.92 ± 0.04), DMACA (0.88 ± 0.05), and PMNet (0.77 ± 0.13). These results sharply contrast with the near-zero performance observed in realistic WSI-level evaluation. This disparity highlights a critical limitation of current methods in practical scenarios where glomerular regions must be automatically identified within complex tissue structures. Although the per-crop results demonstrate technical merit, they offer little scope for meaningful improvement and, more importantly, do not translate into clinically viable solutions for automated global glomerulosclerosis segmentation.

C. Qualitative Analysis

In Figure 3, the visual comparison of FSS model outputs on a zoomed region of a WSI containing three globally sclerotic glomeruli illustrates the difficulty of segmenting these structures at the WSI level. Only HSNet produced meaningful segmentation, successfully identifying and partially segmenting two of the three glomeruli. In contrast, DMACA, VAT, and PMNet failed to generate usable masks, producing only minimal noise-like artifacts indicative of false positives. This qualitative assessment is consistent with the near-zero quantitative performance reported in Table II.

On the other hand, the per-crop analysis of a globally sclerotic glomerulus with HE staining reveals clear differences in segmentation behavior among the four models, as shown in Fig. 4. PMNet produced irregular masks with extensive false negatives, while DMACA achieved more complete coverage but missed pixels mainly along the glomerular borders. VAT further reduced these errors, leaving only scattered omissions, and HSNet showed similarly limited false negatives but introduced small false positives at the boundaries. This segmentation behavior is consistent with the quantitative results, where VAT (0.93 ± 0.03) and HSNet (0.92 ± 0.04) exhibited the best performance, whereas PMNet displayed the lowest and most variable results (0.77 ± 0.13).

IV. Discussion and Concluding Remarks

In this study, we tackled the challenging task of segmenting global glomerulosclerosis. We investigated glomerulus segmentation in WSIs of human kidneys using a FSS approach, evaluating four models: DMACA, VAT, HSNet, and PMNet. Experiments were conducted on three datasets: One containing glomeruli without lesions, another with glomeruli exhibiting segmental and global sclerosis, and a third with glomeruli classified as normal, segmental, or global.

A stark performance gap was observed, particularly for globally sclerotic glomeruli. While models excelled in per-crop analysis, their WSI-level performance collapsed entirely, yielding a Dice score of nearly zero. This failure is attributed to the fundamental challenge of segmenting borderless structures; the absence of a defined Bowman's capsule in globally sclerotic glomeruli renders them indistinguishable from the surrounding interstitial tissue, making automated segmentation an ill-posed problem for current methodologies.

These findings have significant implications for computational nephropathology, demonstrating that common evaluation protocols can severely overestimate a model's real-world utility and misguide clinical deployment decisions. The variability in staining protocols and inherent class imbalance in our datasets further reflects the challenges of clinical practice. Consequently, segmenting globally sclerotic glomeruli remains an open problem. Future work will focus on evaluating foundation models for unsupervised segmentation, enhancing

predictions on human data, and expanding annotated WSI collections to include diverse stains and lesions, ultimately providing a more comprehensive resource for the scientific community.

ACKNOWLEDGMENT

Márcio dos Santos is sponsored by CNPQ under the grant no. 51803. Angelo Duarte is sponsored by FAPESB and UEFS, under the grants PET 0017/2024 and FINAPESQ 074/2021. Luciano Oliveira and Washington LC dos-Santos are sponsored by CNPq under grants 301789/2025-8 and 406141/2023, respectively.

REFERENCES

[1] M. K. K. Niazi, A. V. Parwani, and M. N. Gurcan, "Digital pathology and artificial intelligence," *The lancet oncology*, vol. 20, no. 5, pp. e253–e261, 2019.

[2] V. Della Mea, F. Demichelis, F. Viel, P. Dalla Palma, and C. A. Beltrami, "User attitudes in analyzing digital slides in a quality control test bed: A preliminary study," *Computer Methods and Programs in Biomedicine*, vol. 82, no. 2, pp. 177–186, 2006.

[3] N. Bayramoglu, J. Kannala, and J. Heikkilä, "Deep learning for magnification independent breast cancer histopathology image classification," in *2016 23rd International conference on pattern recognition (ICPR)*. IEEE, 2016, pp. 2440–2445.

[4] M. Haas, S. V. Seshan, L. Barisoni, K. Amann, I. M. Bajema, J. U. Becker, K. Joh, D. Ljubanovic, I. S. Roberts, J. J. Roelofs *et al.*, "Consensus definitions for glomerular lesions by light and electron microscopy: recommendations from a working group of the renal pathology society," *Kidney international*, vol. 98, no. 5, pp. 1120–1134, 2020.

[5] L. Jiang, W. Chen, B. Dong, K. Mei, C. Zhu, J. Liu, M. Cai, Y. Yan, G. Wang, L. Zuo *et al.*, "A deep learning-based approach for glomeruli instance segmentation from multistained renal biopsy pathologic images," *The American Journal of Pathology*, vol. 191, no. 8, pp. 1431–1441, 2021.

[6] A. Jha, H. Yang, R. Deng, M. E. Kapp, A. B. Fogo, and Y. Huo, "Instance segmentation for whole slide imaging: end-to-end or detect-then-segment," *Journal of Medical Imaging*, vol. 8, no. 1, pp. 1–16, 2021.

[7] C. P. Jayapandian, Y. Chen, A. R. Janowczyk, M. B. Palmer, C. A. Cassol *et al.*, "Development and evaluation of deep learning–based segmentation of histologic structures in the kidney cortex with multiple histologic stains," *Kidney International*, vol. 99, no. 1, pp. 86–101, 2021.

[8] N. Bouteldja, B. M. Klinkhammer, R. D. Bülow, P. Droste, S. W. Otten, S. F. von Stillfried, J. Moellmann, S. M. Sheehan, R. Korstanje, S. Menzel *et al.*, "Deep learning–based segmentation and quantification in experimental kidney histopathology," *Journal of the American Society of Nephrology*, vol. 32, no. 1, pp. 52–68, 2021.

[9] N. Altini, M. Rossini, S. Turkevi-Nagy, F. Pesce, P. Pontrelli, B. Prencipe, F. Berloco, S. Seshan, J.-B. Gibier, A. P. Dorado, G. Bueno, L. Peruzzi, M. Rossi, A. Eccher, F. Li, A. Koumpis, O. Beyan, J. Barratt, H. Q. Vo, C. Mohan, H. V. Nguyen, P. A. Cicalese, A. Ernst, L. Gesualdo, V. Bevilacqua, and J. U. Becker, "Performance and limitations of a supervised deep learning approach for the histopathological oxford classification of glomeruli with iga nephropathy," *Computer Methods and Programs in Biomedicine*, p. 107814, 2023.

[10] J. Silva, L. Souza, P. Chagas, R. Calumby, B. Souza, I. Pontes, A. Duarte, N. Pinheiro, W. Santos, and L. Oliveira, "Boundary-aware glomerulus segmentation: toward one-to-many stain generalization," *Computerized Medical Imaging and Graphics*, vol. 100, p. 102104, 2022.

[11] L. Souza, J. Silva, P. Chagas, A. Duarte, W. L.-d. Santos, and L. Oliveira, "Mouse-to-human transfer learning for glomerulus segmentation," *Computer Methods in Biomechanics and Biomedical Engineering: Imaging & Visualization*, pp. 1–10, 2023.

[12] T. de Bel, M. Hermsen, B. Smeets, L. Hilbrands, J. van der Laak, and G. Litjens, "Automatic segmentation of histopathological slides of renal tissue using deep learning," in *Medical Imaging 2018: Digital Pathology*, vol. 10581. International Society for Optics and Photonics, 2018, p. 1058112.

[13] J. N. Marsh, M. K. Matlock, S. Kudose, T.-C. Liu, T. S. Stappenbeck, J. P. Gaut, and S. J. Swamidass, "Deep learning global glomerulosclerosis in transplant kidney frozen sections," *IEEE transactions on medical imaging*, vol. 37, no. 12, pp. 2718–2728, 2018.

[14] M. Hermsen, T. de Bel, M. Den Boer, E. J. Steenbergen, J. Kers, S. Florquin, J. J. Roelofs, M. D. Stegall, M. P. Alexander, B. H. Smith *et al.*, "Deep learning–based histopathologic assessment of kidney tissue," *Journal of the American Society of Nephrology*, vol. 30, no. 10, pp. 1968–1979, 2019.

[15] G. Bueno, M. M. Fernandez-Carrobles, L. Gonzalez-Lopez, and O. Deniz, "Glomerulosclerosis identification in whole slide images using semantic segmentation," *Computer methods and programs in biomedicine*, vol. 184, pp. 1–10, 2020.

[16] N. Altini, G. D. Cascarano, A. Brunetti, F. Marino, M. T. Rocchetti, S. Matino, U. Venere, M. Rossini, F. Pesce, L. Gesualdo *et al.*, "Semantic segmentation framework for glomeruli detection and classification in kidney histological sections," *Electronics*, vol. 9, no. 3, pp. 1–15, 2020.

[17] R. C. Davis, X. Li, Y. Xu, Z. Wang, N. Souma, G. Sotolongo, J. Bell, M. Ellis, D. Howell, X. Shen *et al.*, "Deep learning segmentation of glomeruli on kidney donor frozen sections," *medRxiv*, pp. 1–27, 2021.

[18] J. Gallego, Z. Swiderska-Chadaj, T. Markiewicz, M. Yamashita, M. A. Gabaldon, and A. Gertych, "A u-net based framework to quantify glomerulosclerosis in digitized pas and h&e stained human tissues," *Computerized Medical Imaging and Graphics*, vol. 89, p. 101865, 2021.

[19] L. Yu, M. Yin, R. Deng, Q. Liu, T. Yao, C. Cui, J. Guo, Y. Wang, Y. Wang, S. Zhao *et al.*, "Glo-in-one-v2: holistic identification of glomerular cells, tissues, and lesions in human and mouse histopathology," *Journal of Medical Imaging*, vol. 12, no. 6, pp. 061 406–061 406, 2025.

[20] X. Wang, J. Zhang, Y. Xu, Y. Huang, W. Ming, Y. Jiao, B. Liu, X. Fan, and J. Xu, "Glo-net: A dual task branch based neural network for multi-class glomeruli segmentation," *Computers in Biology and Medicine*, vol. 186, p. 109670, 2025.

[21] J. Min, D. Kang, and M. Cho, "Hypercorrelation squeeze for few-shot segmentation," in *Proceedings of the IEEE/CVF International Conference on Computer Vision (ICCV)*, 2021.

[22] X. Shi, D. Wei, Y. Zhang, D. Lu, M. Ning, J. Chen, K. Ma, and Y. Zheng, "Dense cross-query-and-support attention weighted mask aggregation for few-shot segmentation," in *European Conference on Computer Vision*. Springer, 2022, pp. 151–168.

[23] H. Chen, Y. Dong, Z. Lu, Y. Yu, and J. Han, "Pixel matching network for cross-domain few-shot segmentation," in *Proceedings of the IEEE/CVF Winter Conference on Applications of Computer Vision (WACV)*, January 2024, pp. 978–987.

[24] S. Hong, S. Cho, J. Nam, S. Lin, and S. Kim, "Cost aggregation with 4d convolutional swin transformer for few-shot segmentation," in *European Conference on Computer Vision*. Springer, 2022, pp. 108–126.